Analyst

ROYAL SOCIETY OF CHEMISTRY

PAPER

View Article Online
View Journal | View Issue

Cite this: *Analyst*, 2024, **149**, 1502

Evaluating diverse electrode surface patterns of 3D printed carbon thermoplastic electrochemical sensors†

Chloe Miller,[a,b] Oliver Keattch,[a] Ricoveer S. Shergill[a,b] and Bhavik Anil Patel *[a,b]

Electrochemical sensing techniques rely on redox reactions taking place at the electrode surface. The configuration of this surface is of the utmost importance in the advancement of electrochemical sensors. The majority of previous electrode manufacturing methods, including 3D printing have produced electrodes with flat surfaces. There is a distinct potential for 3D printing to create intricate and distinctive electrode surface shapes. In the proposed work, 3D printed carbon black polylactic acid electrodes with nine different surface morphologies were made. These were compared to a flat surface electrode. To evaluate the performance of the electrodes, measurements were conducted in three different redox probes (ferrocene methanol, ferricyanide, and dopamine). Our findings highlighted that when electrodes were normalised for the geometric surface area of the electrode, the surface pattern of the electrode surface can impact the observed current and electron transfer kinetics. Electrodes that had a dome and flag pattern on the electrode surface showed the highest oxidation currents and had lower values for the difference between the anodic and cathodic peak current (ΔE). However, designs with rings had lower current values and higher ΔE values. These differences are most likely due to variations in the accessibility of conductive sites on the electrode surface due to the varying surface roughness of different patterned designs. Our findings highlight that when making electrodes using 3D printing, surface patterning of the electrode surface can be used as an effective approach to enhance the performance of the sensor for varying applications.

Received 16th September 2023,
Accepted 12th January 2024

DOI: 10.1039/d3an01592k

rsc.li/analyst

Introduction

3D printing is a novel technique that allows for low-cost fabrication of electrodes for a variety of applications such as biological, environmental, and medical.[1–7] The process gives the ability to produce electrochemical sensors of assorted sizes and shapes. Fused Deposition modelling (FDM) is a widely used technique that extrudes thermoplastic materials layer by layer by melting the raw material.[8] The nozzle is heated to the appropriate temperature and the printer allows movement in the *X*, *Y*, and *Z* direction for the print to begin, extruding the material layer by layer until the process is complete. This allows for higher precision and greater uniformity of the printed electrodes, producing a higher reproducibility rate than manufacturing electrodes by hand.[8–10] Electrodes are made using printable filaments that are composed of a conductive material like carbon and non-conductive thermoplastics such as polylactic acid (PLA).[11–13] The resultant electrodes are composite electrochemical sensors.[14–17]

Electrochemical processes such as redox reactions, take place at the surface of the working electrode, and thus the nature of the electrode surface is important.[18] There have been many studies over the years that have explored how changes in the electrode surface can impact the behaviour of the electrode. These have focused on alterations of the surface geometry or changes in surface roughness.[19–24] These studies have shown that having either an ordered or disordered (*e.g.* composite electrodes) electrode surface morphology can increase the surface roughness, which in turn increases the available conductive sites on the electrode surface.[19,20,25] Furthermore, these exposed conductive sites may expose defect sites and edge planes on carbon-based material, which provide access to various terminal functional group (*e.g.*, hydrogen, hydroxyl, carbonyl and carboxyl groups). Such changes can enhance the current response and improve electron transfer kinetics.[26–28] Theoretical studies that have explored the impact of varying nanostructured patterns and electrode surface roughness have showcased that this can significantly alter the shape of cyclic voltammograms and peak currents.[21,29–31]

Studies on carbon fibre microelectrodes have shown that increases in the electrode roughness can expose a higher pro-

[a]*School of Applied Sciences, Brighton, BN2 4GJ, UK.*
E-mail: b.a.patel@brighton.ac.uk
[b]*Centre for Lifelong Health, Brighton, BN2 4GJ, UK*

† Electronic supplementary information (ESI) available: Fig. S1–S6 and Table S1. See DOI: https://doi.org/10.1039/d3an01592k

portion of edge plane sites for adsorption, resulting in enhanced sensitivity for the detection of neurotransmitters.[19] When using carbon thermoplastic electrodes, studies have shown that the type of thermoplastic can influence the degree of surface roughness and edge-plane carbon structures exposed on the electrode surface.[32] Electrodes that had a higher surface roughness and increased edge-plane rich morphology gave a lower capacitance and enhanced redox behaviour.[32,33] These studies have showcased that variation of surface morphology can impact surface roughness, which in turn can affect the electrochemical response. Although studies have been conducted using carbon composite thermoplastic electrodes, these have unordered electrode surface structure. 3D printing can provide the ability to create structured geometry on the electrode surface to understand if specific patterned structures can increase roughness and provide greater access to carbon sites.

This study explores the impact of machine patterned 3D printed carbon black polylactic acid (CB/PLA) electrode surfaces on the electrochemical activity of various redox probes and biological analytes. Topography studies were conducted to understand the differences in surface roughness of the various patterned electrode surfaces. This was followed by studying the sensitivity of the best and worst-performing electrodes in dopamine and serotonin (5-HT). Lastly the electrodes were accessed for their ability to detect 5-HT overflow from colonic tissue.

Experimental

Materials

All chemicals used were of analytical grade and redox probe solutions were prepared with 0.1 M Potassium Chloride (KCl) in deionised water, with dopamine being prepared in 0.1 M PBS, at pH 7.34. Ferrocene Methanol (FcMeOH) and Ferricyanide ($Fe(CN)_6^{3-/4-}$) were bought from Merck (Gillingham, United Kingdom), and KCl was bought from Fisher Scientific (Loughborough, United Kingdom).

Production of the 3D printed CB/PLA electrodes

CB/PLA filament (Proto Pasta, purchased from Filaprint, UK) was used to make 10 mm diameter and 3 mm height electrodes using a Flash Forge Creator Pro printer. The patterned surfaces were designed using CAD as shown in Fig. S1.† The outer casings of the electrodes were printed with orange PLA filament (Raise3D Premium) to fit CB/PLA electrodes with a recess of 2 mm. The electrodes were put in the casing so that the patterned size was in the recess, with the flat side available for making electrical conduct. The electrodes were set to print with an extruder temperature of 230 °C and the heated bed had a temperature of 50 °C. The print layer thickness was 0.1 mm. These parameters were set based on earlier studies conducted.[34,35] The electrical connection was made by attaching a copper wire using conductive silver epoxy (Circuit Works) to the CB/PLA electrodes.[34,36] This was then sealed 24 hours later using a glue gun to form an insulation around the ohmic connection. This only exposes the patterned surface as the sensing side of the electrode.

Electrochemical characterization

A three-electrode system was used to conduct the electrochemical measurements; the counter electrode used was a platinum wire, the reference was Ag|AgCl (3 M KCl) and the working electrode was various 3D printed CB/PLA electrodes with different patterned surfaces. The electrochemical experiments were conducted using a CH1030E potentiostat (CH instruments, Texas). Prior to conducting electrochemical measurements, all electrodes were electrochemically pretreated using 0.5 M Sodium Hydroxide by holding the potential at 1.4 V, then at −1.0 V for 200 seconds each *vs.* Ag|AgCl.[3,37] Cyclic Voltammetry measurements were conducted in 1 mM ferrocene methanol in 1 M KCl with the potential window at −0.5 to +0.6 V *vs.* Ag|AgCl. For experiments conducted in 1 mM ferricyanide in 1 M KCl, the potential window of −0.2 to +0.7 V *vs.* Ag|AgCl. Studies for dopamine were conducted in 1 M KCl at a concentration of 1 mM, with the potential window of −0.2 to +0.8 V *vs.* Ag|AgCl. All the cyclic voltammetric experiments were performed using a scan rate of 50 mV s^{-1}. EIS measurements were carried out using 1 mM ferricyanide and 1 mM ferrocyanide mixture solution 1 M KCl, where the R_{ct} was obtained following fitting the experimental data with a modified Randles equivalent circuit. Amperometry calibrations (2 to 10 μM) for dopamine were conducted in 0.1 M PBS buffer and for serotonin 5-HT in Krebs buffer solution (pH 7.4; 117 mM NaCl, 4.7 mM KCl, 2.5 mM $CaCl_2$, 1.2 mM $MgCl_2$, 1.2 mM NaH_2PO_4, 25 mM $NaHCO_3$ and 11 mM glucose) with the voltage being held at +0.45 *vs.* Ag|AgCl.

Measurements from colonic tissue

All animal procedures were performed in accordance with the Guidelines for Care and Use of Laboratory Animals of the University of Brighton and approved by the University of Brighton Animal Ethics Committee. Male C57/BL6 mice (6–11 weeks) were euthanized using CO_2 gas then dissected to remove the colon. The colon was cut into 2–3 mm segments and placed in Krebs buffer with or without 1 μM fluoxetine within an incubator for 10 minutes. A small aliquot of the supernatant was added to monitor the 5-HT overflow on the different electrodes.

Data analysis

The electrode surface area of the patterned electrodes as shown in Table S1† was obtained by selecting the appropriate surfaces using Rhino software. For cyclic voltammetry measurements, the cathodic and anodic peak potentials, and the difference between the potentials (ΔE) were measured. Additionally, the cathodic and anodic peak currents were recorded and normalised by the electrode surface area. ImageJ was used to obtain the A_b values for the surface roughness from optical microscopy images. Statistical analysis was con-

ducted using GraphPad Prism 8.0, using student *t*-tests and one-way ANOVA.

Results and discussion

Comparison of the electrochemical pre-treated CB/PLA electrodes printed by 3D printer

Fig. S2† shows light microscopy images of the patterned surfaces once they have been printed. Close grid electrode shows slight shrinkage with the square patterning, giving this pattern more of a flat surface compared to the others. The dome pattern is not as clear as it could be, with the individual domes not being distinctly separate. This can also be seen when comparing the grid pattern, indicating that having individual sections on the top layer rather than the whole surface being indented, will result in slight changes occurring. When observing the light microscopy images of the printed and pre-treated electrodes shown in Fig. 1, there are no clear differences between the two, suggesting that using electrochemical pre-treatment does not alter the surface geometry of the electrodes.

Influence of patterned surfaces of CB/PLA electrodes on the response of outer and inner redox probes

The redox probes used were chosen specifically due to their electrochemical properties. FcMeOH is an outer sphere probe that is insensitive to the electrode surface as well as its condition. Fe $(CN)_6^{3-/4-}$ is an inner sphere probe that relies on the electrode surface and whether any metal impurities are present, which influences electron transfer.[37] Fig. 2A shows cyclic voltammograms for the outer sphere redox probe FcMeOH where differences can be seen when comparing the patterned surfaces to the flat surface electrode. In Fig. 2B, the current density (j) for each patterned surface was calculated (using the geometric surface area of the electrode as shown in Table S1†). There were significant increases in j for electrodes with a swirl ($p < 0.01$), domes, square grid, spline rings, and flag patterns (all $p < 0.001$, $n = 6$) when compared to the flat electrode. Electrodes with grid, close grid, smooth rings, and triangle rings pattern were not significantly different from those of the flat electrodes, suggesting that the surface patterns within these electrodes do not provide additive benefits to the performance of the electrode. The ΔE for most electrode surface geometries was lower than that of the flat electrode (Fig. 2C, $p < 0.001$, $n = 6$). No differences in ΔE were observed in smooth rings and triangle rings patterns when compared to the flat electrode. These findings suggest that the addition of a patterned layer on the surface of the electrode improves the electron transfer kinetics and may be due to the increased access to surface carbon electroactive sites, as seen in previous literature.[19,21]

Fig. 2D shows cyclic voltammetry responses of the patterned electrodes for the inner sphere redox probe Fe $(CN)_6^{3-/4-}$ where differences in current response can be seen when compared to the flat surface. Fig. 2E shows that there was a significant increase in the current densities for Fe $(CN)_6^{3-/4-}$ for electrodes with domes, square grid, close grid, triangle rings, swirl, and flag patterned electrodes when compared to flat surface electrodes (all $p < 0.001$, $n = 6$). In a similar fashion to that observed in the outer sphere redox probe, no differences in the current response were observed for grid, smooth rings, and spline rings patterned electrodes when compared to flat

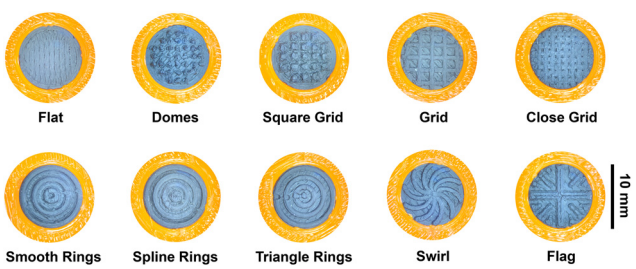

Fig. 1 Microscopy images of the 9 patterned surfaces of the 3D printed CB/PLA electrodes after pre-treatment. The shapes include flat, domes, square grid, grid, close grid, smooth rings, spline rings, triangle rings, swirl, and flag.

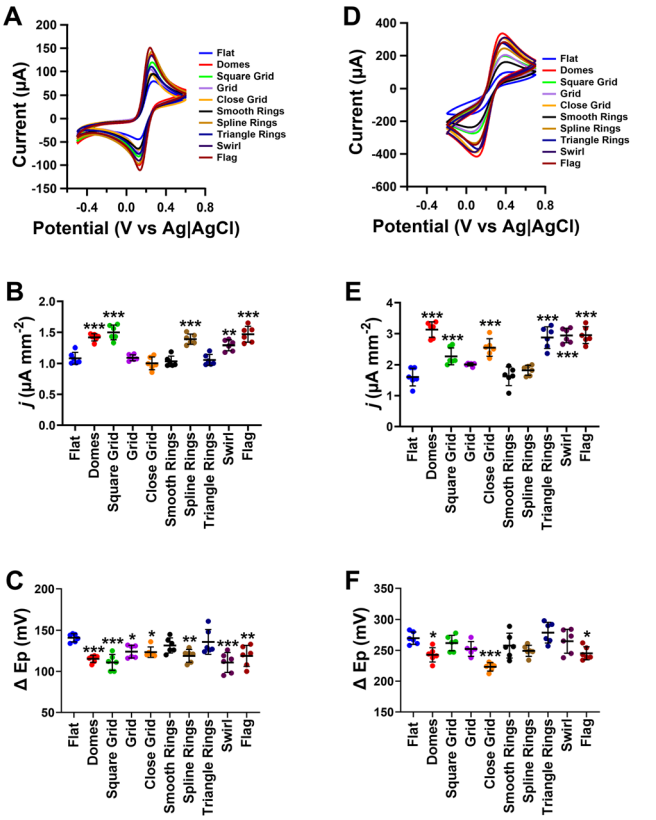

Fig. 2 Responses of outer sphere and inner sphere redox probes on 3D printed CB/PLA electrodes with various patterned surfaces. (A) Cyclic voltammograms obtained in 1 mM FcMeOH in 1 M KCl at 0.05 V s^{-1} where the (B) current density responses and (C) ΔE were obtained. (D) Cyclic voltammograms of 1 mM Ferricyanide in 1 M KCl at 0.05 V s^{-1} where the (E) current density and (F) ΔE were obtained. Data shown as mean ± SD, where $n = 6$, *$p < 0.05$, **$p < 0.01$ and ***$p < 0.001$.

surface electrodes. This highlights that patterning of the electrode can enhance the current response, through the availability of more electroactive sites on the electrode surface with certain patterned surfaces. In Fig. 2F, ΔE responses for most patterns were not significantly different to that of the flat surface electrode. A significant reduction in the ΔE was observed for domes, flag ($p < 0.05$), and close grid ($p < 0.001$) patterned electrodes when compared to flat surface electrodes. These findings indicate that for inner sphere probes, not all the patterned surfaces have a significant impact on the electron transfer kinetics.

Our findings highlight that some patterned surfaces provide enhanced current responses, beyond that expected from the increase in geometric surface area. Electrodes with domes, flag, and swirl patterned surfaces showed enhanced current responses, whilst grid and smooth rings patterned electrodes showed no difference in the current response. This most likely is due to specific patterned surfaces providing increased surface roughness, which in turn increases the available conductive sites on the electrode surface, which have been observed in other studies.[19,20,25] Additionally, given our electrodes were exposed to electrochemical pre-treatment, studies have shown this can create increased surface roughness[38,39] due to the saponification of the PLA from the electrode surface. This effect on patterned electrodes may also vary and provide greater access to edge-plane rich carbon morphology and nanostructure CB sites, which would provide enhanced redox behaviour.

Electrochemical impedance spectroscopy

To further explore the differences in the patterned surface CB/PLA electrodes, electrochemical impedance spectroscopy measurements were conducted. In Fig. 3A, Nyquist plots of the CB/PLA electrodes with various patterned surfaces were obtained, and the interfacial charge-transfer resistance (R_{ct}) was determined (Fig. 3B). Fig. 3B shows that there was a significant decrease in R_{ct} for electrodes with domes ($p < 0.001$), square grid ($p < 0.05$), close grid ($p < 0.01$), swirl ($p < 0.001$), and flag ($p < 0.001$) patterned electrodes when compared to flat surface electrodes ($n = 6$). These findings support those observed for outer and inner sphere redox probes, further supporting that certain surface patterns can provide greater access to conductive carbon sites on the electrode surface, due to increased surface roughness.

Evaluating the impact of CB/PLA patterned surface electrodes for the oxidation of dopamine

Dopamine is oxidised on the electrode surface following adsorption and thus patterned surfaces may have a significant impact on the current observed. Cyclic voltammograms of dopamine on the various patterned surfaces are shown in Fig. 4A. There was a significantly greater current on domes, swirl, and flag patterned electrode surfaces when compared to the flat surface electrode ($p < 0.001$, $n = 6$, Fig. 4B). However, for the other patterned surfaces, the current density was not significantly different from that of the flat surface electrode. As a clear cathodic peak was not observed on all electrodes, the anodic peak potential (E_{pA}) was measured for all electrodes as shown in Fig. 4C. There was a significant decrease in the E_{pA} for triangle rings, swirl, and flag patterned electrodes when compared to the flat surface electrode. No differences were observed for all other patterned electrodes.

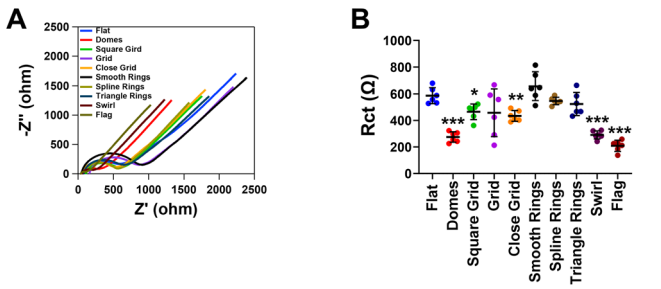

Fig. 3 Electrochemical impedance spectroscopy measurements. (A) Nyquist plots for the electrodes with various patterned surfaces in which the (B) charge-transfer resistance (R_{ct}) was determined. Data are presented as mean ± SD, where $n = 6$, *$p < 0.05$, **$p < 0.01$ and ***$p < 0.001$.

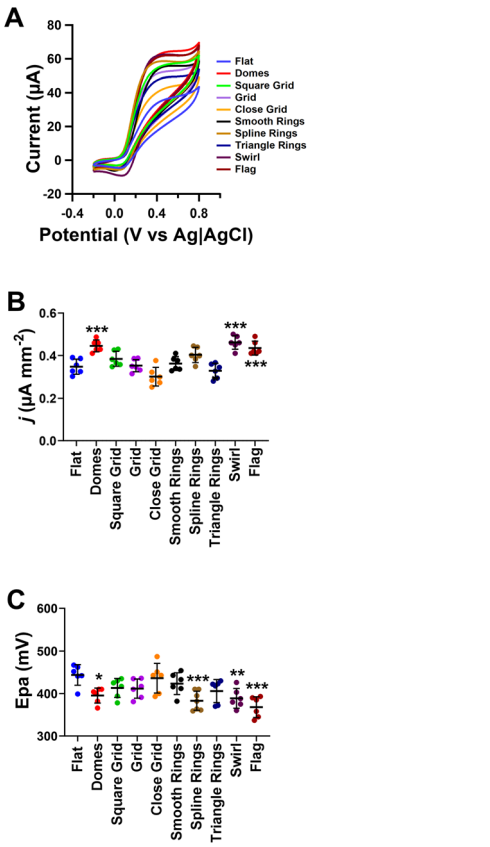

Fig. 4 Responses of 3D printed CB/PLA electrodes with various patterned surfaces in 1 mM Dopamine. (A) Cyclic voltammograms of 1 mM dopamine in 0.1 M PBS at 0.05 V s^{-1}. (B) Current density and (C) anodic peak potential (E_{pA}). Data shown as mean ± SD, where $n = 6$, *$p < 0.05$, **$p < 0.01$ and ***$p < 0.001$.

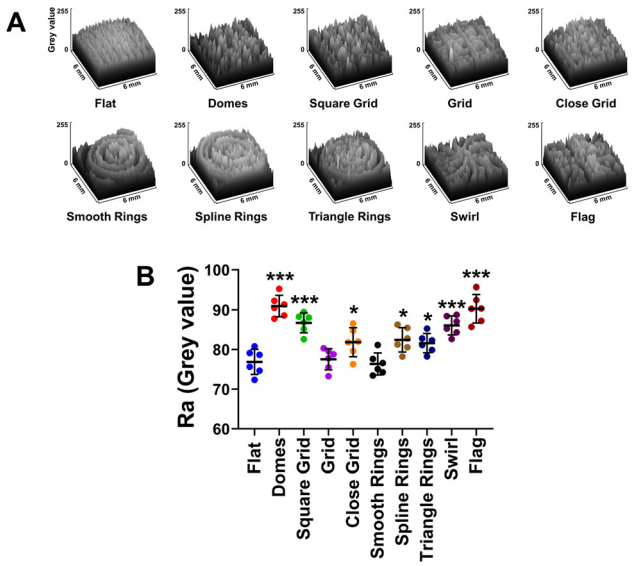

Fig. 5 Surface roughness analysis. (A) The surface profile of a print layer of each pattern. (B) Analysis of the average surface roughness (A_b) measured in grey values obtained from three print layers of the electrodes. Data shown as mean ± SD, where n = 6, *p < 0.05 and ***p < 0.001.

These findings showcase that for adsorption-based redox species, there are some variations in how surface patterned electrodes can impact the current measured, which follow similar patterns to that observed with inner and outer sphere redox probes. Electrodes with patterns of domes and flag provided a greater current response and reduced electron transfer kinetics when compared to the flat surface. Grid and smooth rings patterned electrodes however, had no differences in performance to flat surface electrodes. Therefore, this highlights that certain patterning can have an influence on the performance of the electrode.

Surface roughness

To gain a further understanding of why such differences in the performance of the electrodes with varying surface patterns occurred, the roughness of the electrode surface was measured. Fig. 5A shows the surface profile of a 6 by 6 mm segment of the electrode surface, where clear variations in the different surface patterns occurred. The average surface roughness (R_a), when accounting for surface shape was obtained, where smaller values indicate a smoother surface and larger values indicate a rougher surface. This shows that certain surface patterns have a more distinct surface roughness compared to others, in which these trends closely followed those observed for the responses on the various redox probes. Close grid, spline rings, triangle rings (all with $p < 0.05$), domes, square grid, swirl, and flag (all with $p < 0.001$) all had significantly higher A_b values when compared to the flat surfaced electrode (n = 6) However, the remaining shapes (grid and smooth rings) did not have an increased surface roughness, indicating printing of these patterns or electrochemical treatment of these patterns did not increase additional surface roughness. Fig. S3† shows that the electrode roughness is correlated with j values for the various redox probes and R_{ct} values on the different patterned electrodes. These findings showcase that shapes with more linear largest peak-to-valley amplitude patterns have an increased surface roughness and therefore are more likely to provide greater access to conductive sites on the electrode surface, providing an improved electrochemical behaviour.

Evaluating which patterned electrode surface provides the most enhanced performance for the detection of redox species

To understand which patterned electrode surface provided the best and worst overall performance, the response from measurements of all the redox probes was conducted. Statistical analysis comparing all the different patterned electrode surfaces in the different redox probes is shown in Fig. S4.† Table 1 shows the overall performance of the electrodes in the three redox probes and EIS measurements. The worst performing electrodes are shown in red, whilst the best performing electrodes are shown in green. Flag and dome patterned electrodes gave the best performance, with the highest j values, low R_{ct} values, lowest ΔE values for FcMeOH and Fe$(CN)_6^{3-/4-}$ and lowest E_{pA} values for dopamine. Smooth rings and grid patterned electrodes gave the worst performance with the lowest j values and poor electron transfer kinetics when compared to all other patterned surfaces.

Table 1 Results to show a comparison of the performances of the electrodes in the redox probes used. The colour of the cell indicates the strength of the performance, where green is the best and red is the worst performance. Data is shown as mean, n = 6

	Ferrocene methanol		Ferricyanide		EIS	Dopamine	
	j (μA mm^{-2})	ΔE (mV)	j (μA mm^{-2})	ΔE (mV)	R_{ct} (ohms)	j (μA mm^{-2})	E_{pA} (mV)
Domes	1.42	115	3.13	243	275.2	0.45	405
Square grid	1.50	111	2.27	262	465.2	0.39	413
Grid	1.09	124	2.01	252	457.7	0.35	421
Close grid	1.00	123	2.55	223	434.0	0.30	436
Smooth rings	1.03	132	1.63	258	656.8	0.36	431
Spline rings	1.39	119	1.82	249	546.3	0.40	379
Triangle rings	1.06	136	2.88	279	523.8	0.33	406
Swirl	1.29	111	2.93	265	291.0	0.46	389
Flag	1.47	119	2.95	245	208.7	0.43	380

Table 1 shows there is no specific pattern which shows enhanced performance of all types of redox probes; however, flag and dome patterned electrodes generally perform well, whilst smooth rings electrodes do not perform well. These findings indicate that depending on the type of electroanalytical sensing approach, specific pattern surfaces can offer improved performance. For inner sphere probes, square draft performs the best, for outer sphere probes, dome patterned electrodes are best and for adsorption-based systems swirl and flag patterns are best performing patterns. These variations must be associated with the degree of surface roughness, accessibility of conductive sites and importantly the degree of edge-plane carbon sites accessible on the electrode surface.

Comparing the analytical performance of CB/PLA electrodes with smooth rings and flag patterned surfaces

The analytical performance of the electrodes was assessed using dopamine and serotonin, which are important neurotransmitters. Measurements were conducted using the best (flag pattern) and worst (smooth rings pattern) performing patterned surfaces. Fig. S5A† shows current responses for dopamine in concentrations from 2–10 μM. Fig. S5B† shows that flag patterned electrodes produced a greater current response when compared to smooth rings patterned electrodes ($p < 0.001$, $n = 5$). The limit of detection (LOD, defined as 3 times the deviation of the slope from the standard error of the calibration response) was 0.36 μM and the sensitivity was 0.22 μM μA^{-1} for the flag pattern electrode. The LOD was 0.72 μM and the sensitivity was 0.07 μM μA^{-1} for the smooth rings patterned electrode. These differences in the sensitivity and LOD of the two patterned electrodes highlight that surface patterning of the electrode can have a dramatic impact on the performance of the electrochemical sensor.

Measurements were also conducted using 5-HT as shown in Fig. 6, where again there was a significant increase in the current response with increasing concentration on the flag patterned electrode when compared to the smooth rings patterned electrode (Fig. 6B, $p < 0.001$, $n = 4$). To assess the electrodes, measurements were conducted to monitor the serotonin overflow from colonic tissue segment on both patterned electrodes. Fig. 6C, shows the clear increase in the current when the supernatant from incubated colonic tissue was added after 40 s on both electrodes. Fig. 6D shows a significant increase in the amount of 5-HT observed on the flag patterned electrode when compared to the smooth rings patterned electrode ($p < 0.001$, $n = 4$). Fig. S6† shows that on the flag patterned electrode, there was a significant increase in serotonin in the presence of serotonin reuptake inhibitor fluoxetine ($p < 0.001$, $n = 4$). These results further highlight the impact of surface patterns on the electroanalytical performance of electrochemical sensors for bioanalytical measurement.

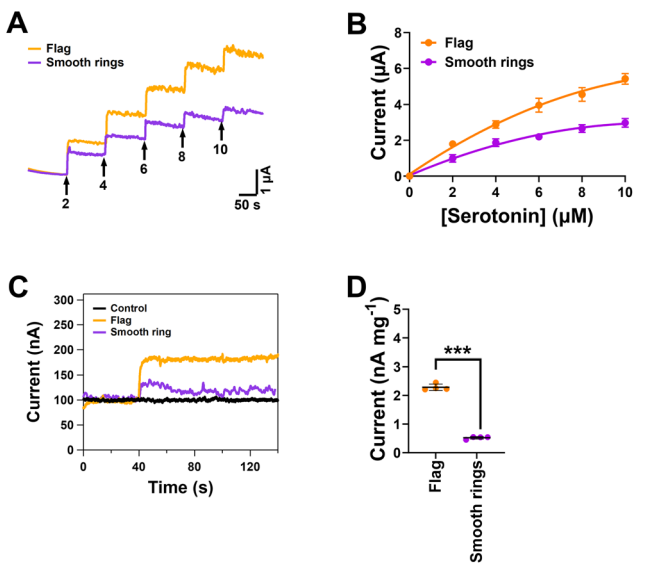

Fig. 6 Calibration of serotonin (5-HT) and measurements from colonic tissue on smooth rings and flag patterned electrodes. (A) Individual amperometric traces showing the change in the current following the addition of 5-HT every 100 seconds. Values are shown in μM with the voltage being held at 0.45 V. (B) Calibration response of flag and smooth rings patterned electrodes. (C) Responses of supernatants, which are added after 40 s from colonic tissue and (D) differences in responses obtained from flag and smooth rings patterned electrodes. Data is shown as mean ± SD, $n = 4$, ***$p < 0.001$.

Conclusions

The work presented shows that machine patterned 3D printed electrodes have an impact on the electrochemical response. No one pattern is ideal for the measurement of all redox probes, but specific patterns show enhanced performance for the measurement of inner sphere, outer sphere or adsorption based redox probes. These variations in performance are due to how different surface patterns can vary the degree of roughness which can in turn influence the number of conductive sites and degree of edge-plane carbon sites on the surface of the electrode. Our findings highlight that surface patterning can have a significant impact on the electrochemical activity of 3D printed electrodes and should be considered when tailoring design of 3D printed electrodes for sensing applications.

Author contributions

C. M.: methodology, investigation, validation, formal analysis, writing – original draft. O. K.: design of surface patterns, R. S. S.: investigation. B. A. P.: conceptualization, methodology, resources, formal analysis, writing – review and editing, supervision, project administration.

Conflicts of interest

There are no conflicts to declare.

Acknowledgements

The authors would like to thank EPSRC (EP/V028391/1) for funding that supported this study.

References

1 Q. Li, J. Zhang, Q. Li, G. Li, X. Tian, Z. Luo, F. Qiao, X. Wu and J. Zhang, *Front. Mater.*, 2019, **5**, 77.
2 R. M. Cardoso, C. Kalinke, R. G. Rocha, P. L. dos Santos, D. P. Rocha, P. R. Oliveira, B. C. Janegitz, J. A. Bonacin, E. M. Richter and R. A. A. Munoz, *Anal. Chim. Acta*, 2020, **1118**, 73–91.
3 E. M. Richter, D. P. Rocha, R. M. Cardoso, E. M. Keefe, C. W. Foster, R. A. A. Munoz and C. E. Banks, *Anal. Chem.*, 2019, **91**, 12844–12851.
4 C. Gonçalves, I. C. Gonçalves, F. D. Magalhães and A. M. Pinto, *Polymers*, 2017, **9**, 269.
5 G. D. O'Neil, *Curr. Opin. Electrochem.*, 2020, **20**, 60–65.
6 A. Ambrosi and M. Pumera, *Chem. Soc. Rev.*, 2016, **45**, 2740.
7 C. L. Manzanares Palenzuela and M. Pumera, *TrAC, Trends Anal. Chem.*, 2018, **103**, 110–118.
8 R. B. Kristiawan, F. Imaduddin, D. Ariawan, Ubaidillah and Z. Arifin, *Open Eng.*, 2021, **11**, 639–649.
9 C. Y. Foo, H. N. Lim, M. A. Mahdi, M. H. Wahid and N. M. Huang, *Sci. Rep.*, 2018, **8**, 7399.
10 R. S. Shergill, C. L. Miller and B. A. Patel, *Sci. Rep.*, 2023, **13**, 339.
11 H. H. Hamzah, S. A. Shafiee, A. Abdalla and B. A. Patel, *Electrochem. Commun.*, 2018, **96**, 27.
12 K. K. Hussain, R. S. Shergill, H. H. Hamzah, M. S. Yeoman and B. A. Patel, *ACS Appl. Polym. Mater.*, 2023, **5**, 4136–4145.
13 M. H. Omar, K. A. Razak, M. N. Ab Wahab and H. H. Hamzah, *RSC Adv.*, 2021, **11**, 16557–16571.
14 P. Awasthi and S. S. Banerjee, *Addit. Manuf.*, 2021, **46**, 102177.
15 R. S. Shergill, F. Perez, A. Abdalla and B. A Patel, *J. Electroanal. Chem.*, 2022, **905**, 115994.
16 Y. Ni, R. Ji, K. Long, T. Bu, K. Chen and S. Zhuang, *Appl. Spectrosc. Rev.*, 2017, **52**, 623–652.
17 P. K. Penumakala, J. Santo and A. Thomas, *Composites, Part B*, 2020, **201**, 108336.
18 A. J. Bard, L. R. Faulkner and H. S. White, *Electrochemical methods: fundamentals and applications*, John Wiley & Sons, 2022.
19 Q. Cao, D. K. Hensley, N. V. Lavrik and B. J. Venton, *Carbon*, 2019, **155**, 250–257.
20 Q. Cao, Z. Shao, D. K. Hensley, N. V. Lavrik and B. J. Venton, *Langmuir*, 2021, **37**, 2667–2676.
21 D. Menshykau, I. Streeter and R. G. Compton, *J. Phys. Chem. C*, 2008, **112**, 14428–14438.
22 K. R. Ward, M. Gara, N. S. Lawrence, R. S. Hartshorne and R. G. Compton, *J. Electroanal. Chem.*, 2013, **695**, 1–9.
23 K. R. Ward, N. S. Lawrence, R. S. Hartshorne and R. G. Compton, *Phys. Chem. Chem. Phys.*, 2012, **14**, 7264–7275.
24 A. J. Arvia, R. C. Salvarezza and J. M. Vara, *Electrochim. Acta*, 1992, **37**, 2155–2167.
25 W. Xu, W. J. Chappell, R. G. Cooks and Z. Ouyang, *J. Mass Spectrom.*, 2009, **44**, 353–360.
26 A. Parveen and R. Kant, *J. Phys. Chem. C*, 2014, **118**, 26599–26612.
27 R. Kant, *J. Phys. Chem. C*, 2010, **114**, 10894–10900.
28 P. Leuaa, D. Priyadarshani, A. K. Tripathi and M. Neergat, *J. Electroanal. Chem.*, 2020, **878**, 114590.
29 P. Zhu and Y. Zhao, *Mater. Chem. Phys.*, 2019, **233**, 60–67.
30 M. Arenz, K. J. J. Mayrhofer, V. Stamenkovic, B. B. Blizanac, T. Tomoyuki, P. N. Ross and N. M. Markovic, *J. Am. Chem. Soc.*, 2005, **127**, 6819–6829.
31 S. Dhillon and R. Kant, *Appl. Surf. Sci.*, 2013, **282**, 105–114.
32 C. P. McCord, B. Summers and C. S. Henry, *Electrochim. Acta*, 2021, **393**, 139069.
33 K. J. Klunder, Z. Nilsson, J. B. Sambur and C. S. Henry, *J. Am. Chem. Soc.*, 2017, **139**, 12623–12631.
34 R. S. Shergill and B. A. Patel, *ChemElectroChem*, 2022, **9**, e202200831.
35 J. S. Stefano, L. R. G. e. Silva and B. C. Janegitz, *Microchimica Acta*, 2022, **189**(11), 414.
36 R. S. Shergill, P. Bhatia, L. Johnstone and B. A. Patel, *ACS Sustainable Chem. Eng.*, 2024, **12**, 416–422.
37 M. Wehrhold, T. Neubert, A. Yadav, M. Vondracek, R. Iost, J. Honolka and K. Balasubramanian, *Nanoscale*, 2019, **11**, 14742–14756.
38 R. S. Shergill and B. A. Patel, *ACS Appl. Electron. Mater.*, 2023, **5**, 5120–5128.
39 D. M. Wirth, M. J. Sheaff, J. V. Waldman, M. P. Symcox, H. D. Whitehead, J. D. Sharp, J. R. Doerfler, A. A. Lamar and G. LeBlanc, *Anal. Chem.*, 2019, **91**, 5553–5557.